MECHANIKA TEORETYCZNA
I STOSOWANA
Journal of Theoretical
and Applied Mechanics
2, 31, 1993

LINEAR STABILITY THEORY OF THREE DIMENSIONAL SUPERSONIC BOUNDARY LAYER

EWA SZNITKO

Technical University of Poznań

The linear stability theory is used for investigating the transition phenomena in a three-dimensional supersonic boundary layer induced on a cone rotating in an external flow. The stability equations are solved to determine the eigenvalues, using the compact two-point fourth-order finite-difference scheme. The effect of wall cooling on critical Reynolds number is tested.

1. Introduction

The increasing cost of petroleum products and their reduced availability in the future create new requirements in the design of aircrafts. These requirements make the drag reduction problem to be of paramount importance particularly, in the case of large supersonic aircrafts. At any speed, the principal drag reduction possibilities lie in the maximal stabilization of the laminal boundary layer. By minimizing the growth of linear disturbances, laminar flow can be obtained over a portion of the surface of an aircraft. Such "stability modifiers" as suction, exploitation of favorable pressure gradient, wall cooling and wave cancellation can potentially provide a significant drag reduction by reducing the skin friction over a portion of the surface of an aircraft. The consistent feature of the three-dimansional (3D) boundary layer is the presence of spiral vortices in the laminar-turbulent transition region, which are caused by the crossflow velocity component occurring in the 3D-boundary layer. The critical issue for the control of the laminar-turbulent transition consists in investigations of the stability characteristics of crossflow spiral vortices. A convenient starting point for such investigations can be the boundary layer of a rotating cone. This model problem, exhibiting the same rich variety of instabilities as the swept wing, allows for simpler application of theory and experiments. Based on such studies, hypothesis can be made on a swept wing flow.

The first experimental studies of the crossflow instability in the boundary layer of rotating disk (special case of cone) were carried out by Smith (1946), Gregory et al. (1955). Kobayashi (1981) pioneered the theoretical studies of the stability of rotating cone boundary layer and his investigations were continued by Kobayashi and Izumi (1983). Kohama and Kobayashi (1983) pointed out that on a rotating cone surface there existed two kinds of spiral vortices: counterrotating vortices which took place for the cone angle Θ between $0° \div 30°$ and corotating spiral vortices for angle of the cone between $30° \div 90°$. The schematic picture of counterrotating and corotating vortices is shown in Fig.1.

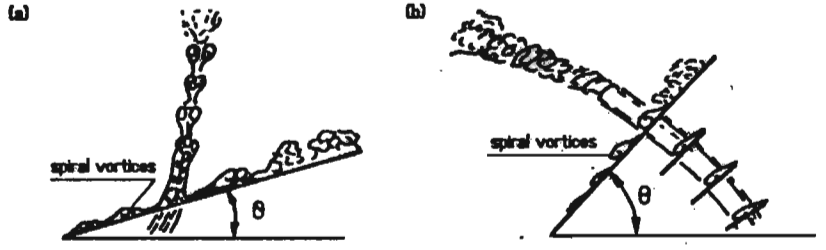

Fig. 1. Schematic picture of counterrotating (a) and corotating (b) spiral vortices

The effect of wall cooling on the stability of the two-dimensional (2D) boundary layer was investigated for the first time by Lees (1947). He found that wall cooling stabilized 2D-disturbances in a flat plate boundary layer. This stabilization takes place because the cooling through the wall temperature lowering, decreases the viscosity close to the wall, which results in a thinner (more stable) boundary layer. Mack (1975) found that wall cooling stabilizes the first mode but destabilizes the higher order modes which appear when the mean flow relative to the phase velocity becomes supersonic. Lekoudis (1979) studied the influence of cooling on 3D-subsonic-transonic boundary layer. He found that wall cooling stabilized the crossflow waves in a subsonic-transonic range of speed. However this stabilization turns out to be relatively small compared with the stabilization which cooling has on Tollmien-Schlichting waves. Balacumar and Reed (1989) investigated wall cooling in supersonic boundary layer.

In the present work the instability characteristics of 3D-supersonic boundary layer induced on the rotating cone surface are investigated theoretically. The effect of wall cooling on crossflow instability is analyzed.

2. Governing equations

We consider a cone rotating around the axis of symmetry with a constant

angular speed Ω in external supersonic flow. The cartesian (x_1, x_2, x_3) and body oriented (ξ, ζ, η) coordinate systems used in this paper are shown in Fig.2, respectively.

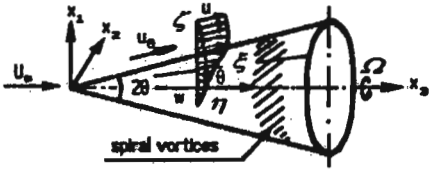

Fig. 2. Schematic picture of rotating cone

The equations governing the flow of a viscous compressible ideal gas (the Navier-Stokes equations, continuity equation and energy equation) can be written in the following form

$$\frac{\partial \mathbf{U}_1}{\partial t} + \frac{\partial \mathbf{E}_1}{\partial \xi} + \frac{\partial \mathbf{F}_1}{\partial \eta} + \frac{\partial \mathbf{G}_1}{\partial \zeta} = \mathbf{0} \tag{2.1}$$

$$\mathbf{U}_1 = \frac{\mathbf{U}^*}{J}$$

$$\mathbf{E}_1 = \frac{1}{J}(\mathbf{E}^*\xi_x + \mathbf{F}^*\xi_y + \mathbf{G}^*\xi_z)$$

$$\mathbf{F}_1 = \frac{1}{J}(\mathbf{E}^*\eta_x + \mathbf{F}^*\eta_y + \mathbf{G}^*\eta_z)$$

$$\mathbf{G}_1 = \frac{1}{J}(\mathbf{E}^*\zeta_x + \mathbf{F}^*\zeta_y + \mathbf{G}^*\zeta_z)$$

$$\mathbf{U}^* = \begin{bmatrix} \rho \\ \rho v_1 \\ \rho v_2 \\ \rho v_3 \\ E_t \end{bmatrix}$$

$$\mathbf{E}^* = \begin{bmatrix} \rho v_1 \\ \rho v_1 v_1 - \delta_{11} + p \\ \rho v_1 v_2 - \delta_{12} \\ \rho v_1 v_3 - \delta_{13} \\ (E_t + p)v_1 - v_1\delta_{11} - v_2\delta_{12} - v_3\delta_{13} + q_1 \end{bmatrix}$$

$$\mathbf{F}^* = \begin{bmatrix} \rho v_2 \\ \rho v_1 v_2 - \delta_{12} \\ \rho v_2 v_2 - \delta_{22} + p \\ \rho v_2 v_3 - \delta_{23} \\ (E_t + p)v_2 - v_1\delta_{12} - v_2\delta_{22} - v_3\delta_{23} + q_2 \end{bmatrix}$$

$$\mathbf{G}^* = \begin{bmatrix} \rho v_3 \\ \rho v_1 v_3 - \delta_{13} \\ \rho v_2 v_3 - \delta_{23} \\ \rho v_3 v_3 - \delta_{33} + p \\ (E_t + p)v_3 - v_1\delta_{13} - v_2\delta_{23} - v_3\delta_{33} + q_3 \end{bmatrix}$$

$$E_t = \rho\Big(e + \frac{v_1^2 + v_2^2 + v_3^2}{2}\Big)$$

$$\xi_x = \cos\Theta \qquad \xi_y = \sin\Theta\sin\eta \qquad \xi_z = \sin\Theta\cos\eta$$

$$\eta_x = 0 \qquad \eta_y = \frac{\cos\Theta}{R} \qquad \eta_z = -\frac{\sin\eta}{R}$$

$$\zeta_x = -\sin\Theta \qquad \zeta_y = \cos\Theta\sin\eta \qquad \zeta_z = \cos\Theta\cos\eta$$

$$J = \frac{1}{R}$$

$$\delta_{ij} = \mu\Big(\frac{\partial v_i}{\partial x_j} + \frac{\partial v_j}{\partial x_i}\Big) - \frac{2}{3}\mu\frac{\partial v_i}{\partial x_i} \qquad i,j = 1,2,3$$

In the above equations

R – distance from the axis of the cone to a point (x_1, x_2, x_3)

$$R = \xi\sin\Theta + \zeta\cos\Theta \tag{2.2}$$

q – heat transfer

$$q = -\lambda\nabla\tau \tag{2.3}$$

v_1, v_2, v_3 – velocity components in x_1, x_2, x_3 directions respectively,

ρ – density,

τ – temperature,

e – specific internal energy,

μ – coefficient of viscosity,

λ – thermal conductivity.

As mentioned above, the spiral vortices appear in the laminar-turbulent transition region of the 3D-boundary layer. We assume that spiral vortices appear as small disturbances when a laminar boundary layer becomes unstable.

Let u, v, w be the velocity components in the ξ, ζ, η directions respectively. The flow parameters $(u^*, v^*, w^*, \tau^*, \rho^*, p^*, \mu^*)$ are described as a sum of mean flow terms $(U, V, W, T, \rho, P, \mu)$ and small disturbance terms $(u', v', w', \tau', \rho', p', \mu')$. The algorithm for mean flow calculations is analized in Section 4. Assuming the flow to be locally parallel, we can describe the flow parameters in the following way

$$u^* = U(\bar{\zeta}) + u' = U(\bar{\zeta}) + \bar{u}(\bar{\zeta})e^{i(\alpha\bar{\xi} + m\eta - \omega t)}$$

$$v^* = v' = \bar{v}(\bar{\zeta})e^{i(\alpha\bar{\xi} + m\eta - \omega t)}$$

$$
\begin{aligned}
w^* &= W(\bar{\zeta}) + w' = W(\bar{\zeta}) + \bar{w}(\bar{\zeta})e^{i((\alpha\bar{\xi}+m\eta-\omega t)} \\
p^* &= P(\bar{\zeta}) + p' = P(\bar{\zeta}) + \bar{p}(\bar{\zeta})e^{i(\alpha\bar{\xi}+m\eta-\omega t)} \\
\tau^* &= T(\bar{\zeta}) + \tau' = T(\bar{\zeta}) + \bar{\tau}(\bar{\zeta})e^{i(\alpha\bar{\xi}+m\eta-\omega t)} \\
\rho^* &= \rho(\bar{\zeta}) + \rho' = \rho(\bar{\zeta}) + \bar{\rho}(\bar{\zeta})e^{i(\alpha\bar{\xi}+m\eta-\omega t)} \\
\mu^* &= \mu(\bar{\zeta}) + \mu' = \mu(\bar{\zeta}) + \bar{\mu}(\bar{\zeta})e^{i(\alpha\bar{\xi}+m\eta-\omega t)}
\end{aligned}
\tag{2.4}
$$

where the parameters $u^*, v^*, w^*, p^*, \tau^*, \rho^*, \mu^*$ are normalized with respect to the free stream values $U_e, U_e^2\rho, T_e, \rho_e, \mu_e$, respectively. The coordinates $\bar{\xi}, \bar{\zeta}$ are normalized with the viscous scale $\sqrt{\nu\xi/U_e}$. The subscript e refers to the conditions at the edge of the boundary layer. In the above equations α and m are the $\bar{\xi}$ and η components of the dimensionless wavenumber vector $\bar{k}$, ω is the dimensionless frequency and $\bar{u}(\zeta), \bar{v}(\zeta), \bar{w}(\zeta), \bar{p}(\zeta), \bar{\tau}(\zeta), \bar{\rho}(\zeta), \bar{\mu}(\zeta)$ are amplitudes of disturbances (the complex functions).

The viscosity μ is assumed to vary according to the Sutherland's formula

$$
\mu = T^{\frac{3}{2}}\left(\frac{1+C}{T+C}\right) \qquad C = \frac{110.4\text{K}}{T_e} \tag{2.5}
$$

Viscosity is the function of temperature only, so its fluctuations can be written in the form (Malik et al., 1982)

$$
\mu' = \frac{d\mu}{dT}\tau' \tag{2.6}
$$

Substituting the expressions (2.4) ÷ (2.6) into the normalized form of governing equations (2.1), we obtain the following ordinary differential equations

$$
(\mathbf{A}D^2 + \mathbf{B}D + \mathbf{C})\Phi = \mathbf{0} \tag{2.7}
$$

where: $D = d/d\zeta$, $\Phi = [\bar{u}, \bar{v}, \bar{w}, \bar{\tau}, \bar{p}]^T$ is a vector of the complex functions, and $\mathbf{A}, \mathbf{B}, \mathbf{C}$ are $[5 \times 5]$ matrices.

The boundary conditions on the velocity fluctuations are the usual no-slip and no-penetration conditions

$$
\bar{u}(0) = \bar{v}(0) = \bar{w}(0) = 0 \tag{2.8}
$$

For the gas flowing over a solid wall the boundary condition (2.9) refering to the temperature fluctuation is used

$$
\bar{\tau}(0) = 0 \tag{2.9}
$$

Since in supersonic flow waves may propagate to infinity, the implementation of the boundary conditions at the outer edge of the boundary layer needs some

explanations. Over the boundary layer edge the elements of the matrices $\mathbf{A}, \mathbf{B}, \mathbf{C}$ (Eq (2.7)) depend only o $\bar{R}(\bar{\zeta})$ (nondimensionalized value of $R(\zeta)$ – Eq (2.2))

$$\bar{R}(\bar{\zeta}) = \mathrm{Re}\sin\theta + \bar{\zeta}\cos\theta \tag{2.10}$$

At high Reynolds number $\bar{R}(\bar{\zeta})$ becomes large and the variations of $\bar{R}(\bar{\zeta})$ from $\mathrm{Re}\sin\theta$ are very small. So, for a point far from the wall we can take $\bar{R}(\bar{\zeta}) =$ const. In such a case the elements of the matrices of Eq (2.7) become constants and Eq (2.7) can be solved by means of the exponential method. The solution of this system of equations can be written as

$$\begin{bmatrix} \bar{u} \\ \frac{d\bar{u}}{d\bar{\zeta}} \\ \bar{v} \\ \bar{p} \\ \bar{\tau} \\ \frac{d\bar{\tau}}{d\bar{\zeta}} \\ \bar{w} \\ \frac{d\bar{w}}{d\bar{\zeta}} \end{bmatrix} = \sum_{i=1}^{8} C_i q_i e^{r_i \bar{\zeta}} \tag{2.11}$$

where q_i are column vectors. Eliminating solutions physically impossible (with real part of r_i greater than zero) we have at $\bar{\zeta} \to \infty$

$$\begin{bmatrix} \bar{u} \\ \frac{d\bar{u}}{d\bar{\zeta}} \\ \bar{v} \\ \bar{p} \\ \bar{\tau} \\ \frac{d\bar{\tau}}{d\bar{\zeta}} \\ \bar{w} \\ \frac{d\bar{w}}{d\bar{\zeta}} \end{bmatrix} = \sum_{i=1}^{4} C_i q_i e^{r_i \bar{\zeta}} \tag{2.12}$$

Now we have eight equations with four unknowns C_1, C_2, C_3 and C_4. Eliminating C_1, C_2, C_3 and C_4 we obtain four necessary boundary conditions at the far field in terms of $(\bar{u}, \frac{d\bar{u}}{d\bar{\zeta}}, \bar{v}, \bar{p}, \bar{\tau}, \frac{d\bar{\tau}}{d\bar{\zeta}}, \bar{w}, \frac{d\bar{w}}{d\bar{\zeta}})$.

3. The solution technique

The linear compressible stability equations are solved using the fourth order accurate two-point scheme which is derived by means of the Euler-Maclaurin formula

(Malik et al., 1982)

$$\varphi^k - \varphi^{k-1} = \frac{h_k}{2}\left[\frac{d\varphi^k}{d\bar{\zeta}} + \frac{d\varphi^{k-1}}{d\bar{\zeta}}\right] - \frac{h_k^2}{12}\left[\frac{d^2\varphi^k}{d\bar{\zeta}^2} - \frac{d^2\varphi^{k-1}}{d\bar{\zeta}^2}\right] + \mathbf{0}(h_k^5) \tag{3.1}$$

where

$$\varphi^k = \varphi(\bar{\zeta}_k) \qquad h_k = \bar{\zeta}_k - \bar{\zeta}_{k-1}$$

The nodes are distributed so that

$$\bar{\zeta}_k = \frac{M - \frac{k-1}{N}}{1 - \frac{k-1}{N} - \frac{M}{\zeta_e}} \qquad k = 1, 2, ..., N+1 \tag{3.2}$$

where: $N+1$ is the total number of nodes and $\bar{\zeta}_e$ is the location of the boundary layer edge. The scaling parameter M is chosen to be twice the height of the nodal point at which the nondimensional mean profile has the value of 0.5 (cf Balacumar and Reed, 1989; Malik et al., 1982). It was found that for a given number of points such a choice of M yielded maximum accuracy.

To apply scheme (3.1) to equations (2.7) we have to formulate them as a set of the first-order differential equations. We can write them as (cf Malik et al., 1982)

$$\frac{d\varphi_i}{d\bar{\zeta}} = \sum_{j=1}^{8} a_{ij}\varphi_j \qquad i = 1, 2, ..., 8$$

$$\frac{d^2\varphi_i}{d\bar{\zeta}^2} = \sum_{j=1}^{8} b_{ij}\varphi_j \tag{3.3}$$

where

$$\varphi_1 = \bar{u} \qquad \varphi_2 = \frac{d\bar{u}}{d\bar{\zeta}} \qquad \varphi_3 = \bar{v}$$

$$\varphi_4 = \bar{p} \qquad \varphi_5 = \bar{\tau} \qquad \varphi_6 = \frac{d\bar{\tau}}{d\bar{\zeta}}$$

$$\varphi_7 = \bar{w} \qquad \varphi_8 = \frac{d\bar{w}}{d\bar{\zeta}}$$

$$b_{ij} = \frac{da_{ij}}{d\bar{\zeta}} + \sum_{l=1}^{8} a_{il}a_{lj}$$

Finally we can write

$$\varphi_i^k - \frac{h_k}{2}\sum_{j=1}^{8} a_{ij}^k\varphi_j^k + \frac{h_k^2}{12}\sum_{j=1}^{8} b_{ij}^k\varphi_j^k -$$

$$-\left[\varphi_i^{k-1} + \frac{h_k}{2}\sum_{j=1}^{8} a_{ij}^{k-1}\varphi_j^{k-1} + \frac{h_k^2}{12}\sum_{j=1}^{8} b_{ij}^{k-1}\varphi_j^{k-1}\right] = 0 \qquad i = 1, 2, ..., 8 \tag{3.4}$$

Following Cebeci and Bradshaw (1984), the above equations system (3.4) with the boundary conditions can be written in the block-tridiagonal form

$$\mathbf{A}_k\boldsymbol{\varphi}^{k-1} + \mathbf{B}_k\boldsymbol{\varphi}^{k} + \mathbf{C}_k\boldsymbol{\varphi}^{k+1} = \mathbf{H} \tag{3.5}$$

where $\mathbf{A}_k, \mathbf{B}_k, \mathbf{C}_k$ are 8×8 matrices and $\mathbf{H}$ is a 8×1 null matrix so the linear stability theory is now reduced to an eigenvalue problem.

To solve the linear stability equations directly the nonhomogeneous boundary conditions are imposed at the wall. The boundary condition $\varphi_1(0) = \bar{u}(0) = 0$ is replaced by $\varphi_4(0) = \bar{p}(0) = 1$. Matrix $\mathbf{H}$ of equations (3.5) now becomes

$$\mathbf{H} = [0, 0, 0, 1, 0, 0, 0, 0]^{\mathsf{T}} \tag{3.6}$$

This is equivalent to normalizing the eigensolutions by the value of pressure perturbation at the wall. Now Eq (3.5) is nonhomogeneous and nontrivial solutions can be obtained using block elimination method. Newton's method is then used (Eq (3.7)) to iterate on α so that the abandoned boundary condition $\bar{u}(0) = 0$ is satisfied

$$\bar{u}(0) + \frac{\partial \bar{u}(0)}{\partial \alpha}\Delta\alpha = 0 \tag{3.7}$$

The iteration process is fast. Fig.3 illustrates the iteration process obtained in the present paper.

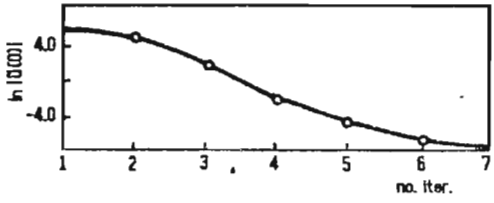

Fig. 3. Illustration of the iteration process (Reynolds number Re = 2000, edge Mach number $\mathrm{Ma}_e = 3.0$, cone angle $\Theta = 15°$)

4. The basic state

The equations of the rotating cone boundary layer can be written in the following way (Balacumar and Reed, 1989; Illingworth, 1953)

$$\frac{\partial(\rho r U)}{\partial \xi} + \frac{\partial(\rho r V)}{\partial \zeta} = 0$$

$$\rho\Big(U\frac{\partial U}{\partial \xi}+V\frac{\partial U}{\partial \zeta}-\frac{WW}{r}\frac{dr}{d\xi}\Big)=\frac{\partial}{\partial \zeta}\Big(\mu\frac{\partial U}{\partial \zeta}\Big)$$

$$\rho\Big(U\frac{\partial(\rho W)}{\partial \xi}+V\frac{\partial(rW)}{\partial \zeta}\Big)=\frac{\partial}{\partial \zeta}\Big(\mu\frac{\partial(rW)}{\partial \zeta}\Big) \tag{4.1}$$

$$\rho\Big(U\frac{\partial h}{\partial \xi}+V\frac{\partial h}{\partial \zeta}\Big)=\frac{1}{\mathrm{Pr}}\frac{\partial}{\partial \zeta}\Big(\mu\frac{\partial h}{\partial \zeta}\Big)+\mu\Big[\Big(\frac{\partial U}{\partial \zeta}\Big)^2+\Big(\frac{\partial W}{\partial \zeta}\Big)^2\Big]$$

$$\rho h=\rho_e h_e$$

Here $r(\xi)$ is the radius of cone at the section ξ, Pr is the Prandtl number which is set to be constant $\mathrm{Pr}=0.72$, and h is enthalpy.

At the wall we have no-slip condition at the impermeable wall and zero heat transfer (i) or isothermal (ii) condition

$$a)\quad \zeta=0:\qquad U=V=0,\qquad W=\Omega r(\xi),\qquad \begin{cases}(i)\quad \frac{\partial h}{\partial \zeta}=0\\ (ii)\quad h=\mathrm{const}\end{cases} \tag{4.2}$$

$$b)\quad \zeta\to\infty:\qquad U=U_e,\qquad V=W=0,\qquad h=h_e$$

The equations are transformed using Mangler's transformation (Cebeci and Bradshaw, 1984)

$$x=\frac{1}{L^2}\int_0^{\xi} r^2(\xi)d\xi=\frac{1}{L^2}\sin^2\Theta\frac{1}{3}\xi^3=\frac{1}{L^2}\sin^2\Theta\frac{1}{3}\frac{\mathrm{Re}^6}{\mathrm{Ro}^6} \tag{4.3}$$

$$y=\frac{r(\xi)\zeta}{L} \tag{4.4}$$

$$\bar{U}=U \tag{4.5}$$

$$\bar{V}=\frac{L}{r}\Big(V+\frac{dr}{d\xi}\frac{1}{r}\zeta U\Big) \tag{4.6}$$

where L is a reference length taken in as a unity for computations. Re and Ro are Reynolds number defined in the following

$$\mathrm{Re}=\sqrt{U_e\frac{\xi}{\nu_e}} \tag{4.7}$$

$$\mathrm{Ro}=\sqrt{U_e\frac{1}{\nu_e}} \tag{4.8}$$

After transformation we obtain

$$\frac{\partial(\rho\bar{U})}{\partial x}+\frac{\partial(\rho\bar{V})}{\partial y}=0$$

$$\rho\bar{U}\frac{\partial\bar{U}}{\partial x}+\rho\bar{V}\frac{\partial\bar{U}}{\partial y}-\rho\frac{WW}{3x}=\frac{\partial}{\partial y}\Big(\mu\frac{\partial\bar{U}}{\partial y}\Big)$$
$$\rho\bar{U}\frac{\partial W}{\partial x}+\rho\bar{V}\frac{\partial W}{\partial y}+\rho\frac{\bar{U}W}{3x}=\frac{\partial}{\partial y}\Big(\mu\frac{\partial W}{\partial y}\Big) \tag{4.9}$$
$$\rho\bar{U}\frac{\partial h}{\partial x}+\rho\bar{V}\frac{\partial h}{\partial y}=\frac{1}{\mathrm{Pr}}\frac{\partial}{\partial y}\Big(\mu\frac{\partial h}{\partial y}\Big)+\mu\Big[\Big(\frac{\partial\bar{U}}{\partial y}\Big)^2+\Big(\frac{\partial W}{\partial y}\Big)^2\Big]$$
$$\rho h=\rho_e h_e$$

The boundary conditions are

$$a)\quad y=0:\qquad \bar{U}=\bar{V}=0\,,\qquad W=\Omega r=\Omega\sqrt[3]{3x\sin\Theta}\,,\qquad \begin{cases}(i)\quad \frac{\partial h}{\partial y}=0\\ (ii)\quad h=\mathrm{const}\end{cases}$$

$$b)\quad y\to\infty:\qquad \bar{U}=U_e\,,\qquad W=\bar{V}=0\,,\qquad h=h_e \tag{4.10}$$

Once again we transform equations in terms of similarity variables

$$\Psi(x,y)=\sqrt{\rho_e\mu_e U_e x}\,f(x,s) \tag{4.11}$$

$$ds=\sqrt{\frac{U_e\rho_e}{\mu_e x}}\frac{\rho}{\rho_e}dy \tag{4.12}$$

Finally the system of boundary layer equations can be written in the following form

$$\frac{\partial}{\partial s}\Big(\mu\rho\frac{\partial^2 f}{\partial s^2}\Big)+\frac{1}{2}f\frac{\partial^2 f}{\partial s^2}-\frac{WW}{3}=x\Big(\frac{\partial f}{\partial s}\frac{\partial^2 f}{\partial x\partial s}-\frac{\partial f}{\partial x}\frac{\partial^2 f}{\partial s^2}\Big)$$
$$\frac{\partial}{\partial s}\Big(\mu\rho\frac{\partial W}{\partial s}\Big)+\frac{1}{2}f\frac{\partial W}{\partial s}-\frac{1}{3}W\frac{\partial f}{\partial s}=x\Big(\frac{\partial f}{\partial s}\frac{\partial W}{\partial x}-\frac{\partial f}{\partial x}\frac{\partial W}{\partial s}\Big) \tag{4.13}$$
$$\frac{\partial}{\partial s}\Big(\mu\rho\frac{\partial h}{\partial s}\Big)+\frac{\mathrm{Pr}}{2}f\frac{\partial h}{\partial s}+\mathrm{Pr}(\kappa-1)\mathrm{Ma}_e^2\mu\rho\Big[\Big(\frac{\partial^2 f}{\partial s^2}\Big)^2+\Big(\frac{\partial W}{\partial s}\Big)^2\Big]=$$
$$=\mathrm{Pr}x\Big(\frac{\partial f}{\partial s}\frac{\partial h}{\partial x}-\frac{\partial f}{\partial x}\frac{\partial h}{\partial s}\Big)$$
$$\rho h=1$$

The boundary conditions are

$$a) \quad s=0: \quad f=\frac{\partial f}{\partial s}=0, \quad W=\frac{\Omega}{U_e}\sqrt[3]{3x\sin\Theta}, \quad \begin{cases} (i) & \frac{\partial h}{\partial s}=0 \\ (ii) & h=\text{const} \end{cases}$$

$$b) \quad s\to\infty: \quad \frac{\partial f}{\partial s}=1, \quad W=0, \quad h=1 \tag{4.14}$$

All parameters in Eqs (4.13) and (4.14) are dimensionless.

To obtain the initial condition for parabolic system of equations (4.13) we expand them in terms of small parameters method (cf Balacumar and Reed, 1989; Illingworth, 1953)

$$e=\Omega\sqrt[3]{3x\sin\Theta} \tag{4.15}$$

$$f=\sum_{n=0}^{\infty}\varepsilon^n f_n(s) \tag{4.16}$$

$$W=\varepsilon\sum_{n=0}^{\infty}\varepsilon^n w_n(s) \tag{4.17}$$

$$h=\sum_{n=0}^{\infty}\varepsilon^n h_n(s) \tag{4.18}$$

After introducing above expressions into Eqs (4.13) and collecting terms, we obtain a system of three equations (4.19) ÷ (4.21) which are solved by the Runge-Kutta scheme and the Newton's method

$$\frac{d}{ds}\Big(\mu\rho\frac{d^2f_0}{ds^2}\Big)+\frac{1}{2}f_0\frac{d^2f_0}{ds^2}=0 \tag{4.19}$$

$$\frac{d}{ds}\Big(\mu\rho\frac{dh_0}{ds}\Big)+\frac{\mathrm{Pr}}{2}f_0\frac{dh_0}{ds}+\mathrm{Pr}(\kappa-1)\mathrm{Ma}_e^2\mu\rho\Big(\frac{d^2f_0}{ds^2}\Big)^2=0 \tag{4.20}$$

$$\frac{d}{ds}\Big(\mu\rho\frac{dw_0}{ds}\Big)+\frac{1}{2}f_0\frac{dw_0}{ds}-\frac{1}{3}\frac{df_0}{ds}w_0=0 \tag{4.21}$$

The boundary conditions are

$$a) \quad s=0: \quad f_0=\frac{df_0}{ds}=0, \quad w_0=1, \quad \begin{cases} (i) & \frac{dh_0}{ds}=0 \\ (ii) & h_0=\text{const} \end{cases} \tag{4.22}$$

$$b) \quad s\to\infty: \quad \frac{df_0}{ds}=1, \quad w_0=0, \quad h_0=1$$

The solution to the system of equations (4.19) ÷ (422), obtained very close to the tip of cone, is used as an initial condition for equation (4.13). The resulting

basic state profiles obtained for $\Omega/U_e = 0.375$, cone angle $\Theta = 15°$ and different edge Mach numbers are shown in Fig.4.

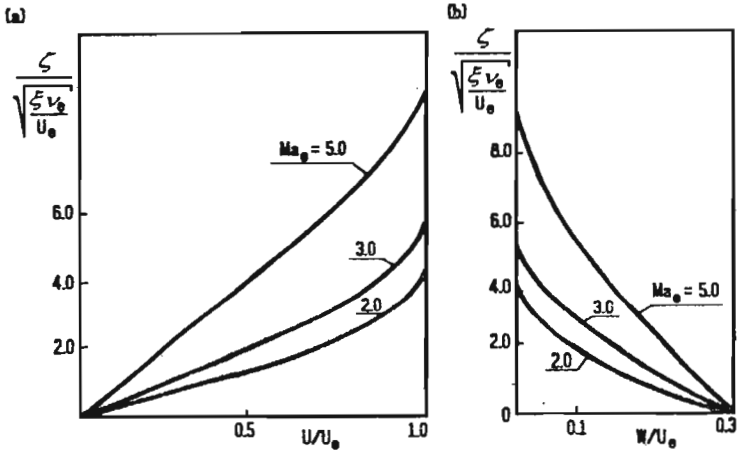

Fig. 4. Basic state profiles (a) streamwise component, (b) azimuthal component

5. Numerical calculations

Numerical calculations were made for two different temperature conditions at the wall: zero heat transfer condition $(\partial T/\partial\bar{\zeta})_w = 0$ (w denotes wall) and isothermal condition $T_w = \text{const}$.

5.1. Zero heat transfer condition at the wall

For the first case solutions were obtained for the following combinations of rotating speed Ω/U_e, edge Mach number Ma_e, Reynolds number Re:

Ω/U_e	Ma_e	Re		
0.000	3.0	1000	2000	3000
0.200	3.0	1000	2000	3000
0.375	3.0	1000	2000	3000
0.500	3.0	1000	2000	3000

In Fig.5a-d, the amplification rate $-\alpha_i$ versus wave number α_r is analyzed. Results are obtained for Reynolds number Re = 2000 and different wave angles

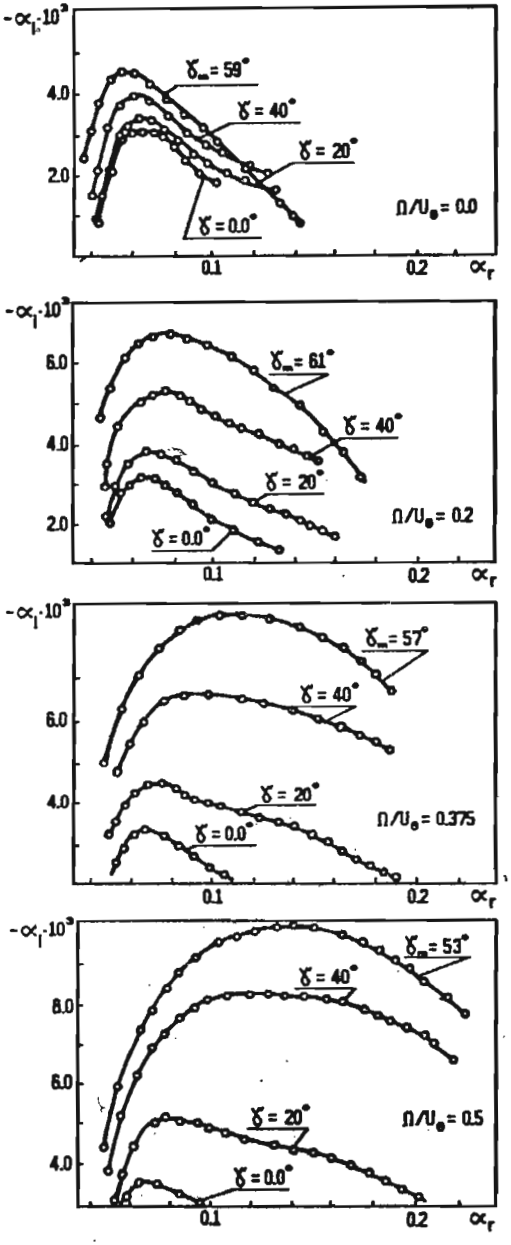

Fig. 5. Instability characteristics obtained for rotational speeds $\Omega/U_e = 0.0$, 0.2, 0.375, 0.5, edge Mach number $\mathrm{Ma}_e = 3.0$, Reynolds number $\mathrm{Re} = 2000$, $\Theta = 15°$ and different wave angles γ

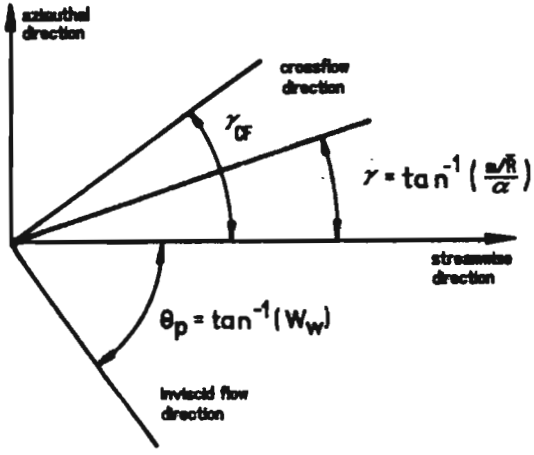

Fig. 6. Schematic diagram of the flow and wave directions, respectively

γ (including the angle of the most unstable wave denoted by γ_m). The wave angle γ is defined by the $\tan\gamma = \beta/\alpha = (m/\bar{R})/\alpha$ (Fig.6). The most unstable crossflow disturbance, according to Owen and Randal (1952) is expected to lie close to the crossflow direction, ie. direction normal to that of the inviscid flow direction. Schematic diagram of the flow and wave directions is shown in Fig.6. The values of the angles γ_m and crossflow angles γ_{CF} are given in Table 1. In Fig.7 the influence of Reynolds number on stability characteristics is shown.

From Fig.5 we see that the amplification rates increase with increasing rotational speed (and with increasing maximum value of crossflow profile). In Table 1 the maximum value of crossflow profile CF_{max} and the crossflow Reynolds number Re_{CF} are shown. When the variables are nondimensionalized by the edge velocity and length scale, the crossflow Reynolds number equals

$$\mathrm{Re}_{CF} = CF_{max}\delta_{10\%}\mathrm{Re} \tag{5.1}$$

where $\delta_{10\%}$ is the distance from the point where the crossflow velocity equals 10% of CF_{max} to the wall. The crossflow profiles obtained for $\mathrm{Ma}_e = 3.0$ and for different rotational speeds are shown in Fig.12 where lines denoted by AD refer to zero heat transfer condition.

The amplification rates (Fig.5) also increase with increasing wave angle and reach the maximum value for angle γ_m. In this paper we restrict our investigations to crossflow disturbances but it is known that when the mean flow relative to the phase velocity becomes supersonic, there exist several unstable modes. In the 3D-boundary layer the amplification rates of the first modes increase while the amplification rates of higher modes decrease with increasing angle from inviscid

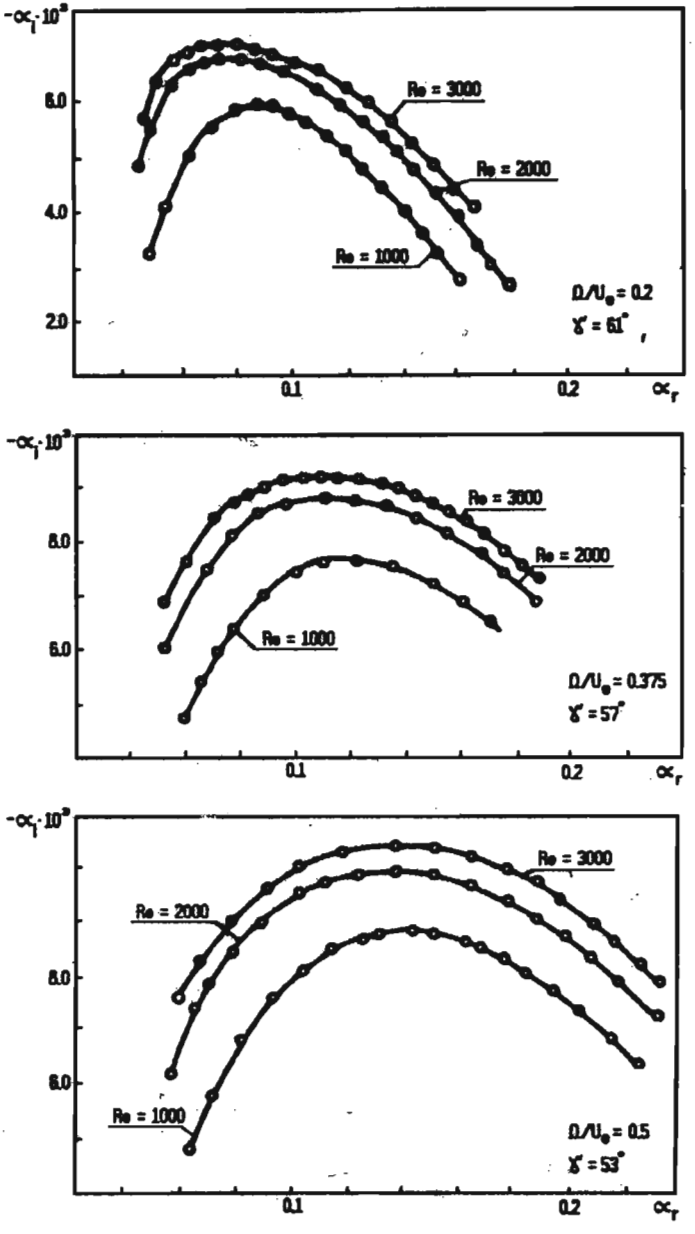

Fig. 7. Instability characteristics obtained for $Ma_e = 3.0$, $\Theta = 15°$ rotational speeds $\Omega/U_e = 0.2$, 0.375, 0.5 and wave angles $\gamma = 61°$, 57°, 53° respectively, and for different Reynolds numbers

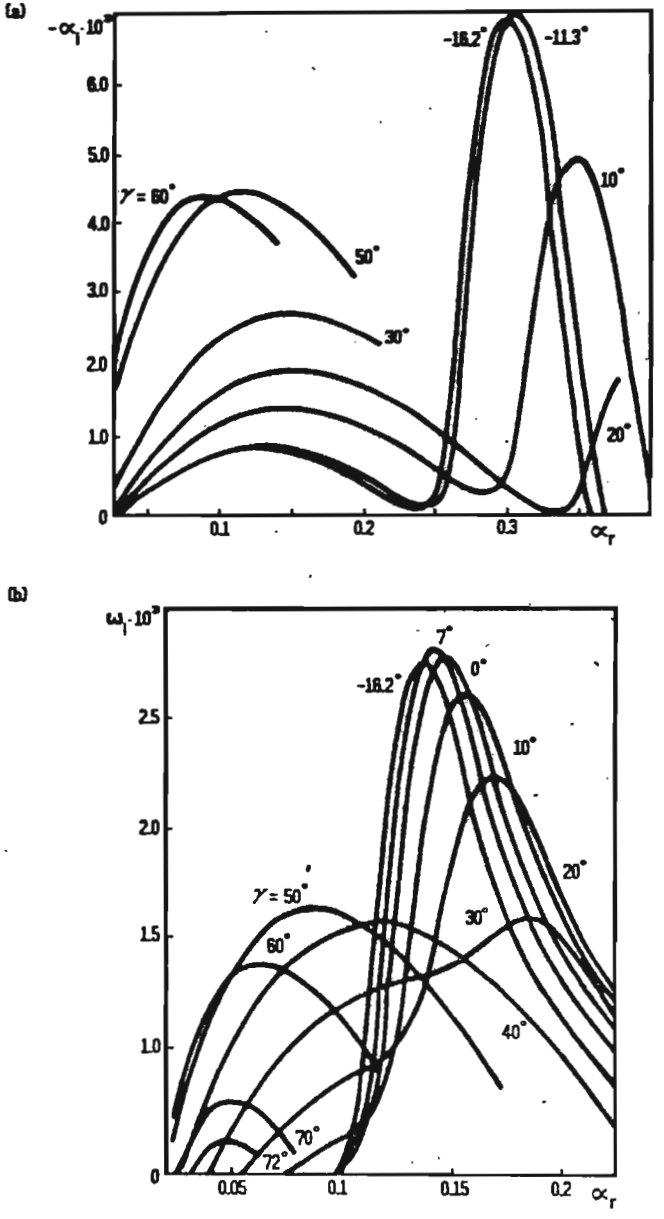

Fig. 8. Instability characteristics obtained for (a) $Ma_e = 5.0$, $Re = 3000$ – spatial theory, for (b) $Ma_e = 8.0$, $Re = 2000$ – temporal theory (Balacumar and Reed, 1989)

flow direction. Fig.8a,b show characteristics obtained by Balacumar end Reed (1989) for $\Omega/U_e = 0.375$, $Ma_e = 5.0$, $Re = 3000$ (spatial theory) and for $\Omega/U_e = 0.375$, $Ma_e = 8.0$, $Re = 2000$ (temporal theory), respectively. It can be seen that for so high Mach numbers the most unstable are waves (second modes) very close to the inviscid flow direction (the angle between the inviscid flow direction and the meridional direction for both cases in Fig.8 is $\Theta_p = -16.2°$). The amplification rates of crossflow disturbances are much smaller than the amplification rates of second modes. The second modes become dominant for the edge Mach number about $Ma_e > 4.0$.

Table 1. The variation of the critical Reynolds number Re_{CR} against crossflow Reynolds number Re_{CF} for different rotational speeds Ω/U_e

Ω/U_e	γ_m	γ_{CF}	Re_{CR}	CF_{max}	Re_{CF}
0.000	59.0°	–	357.0	–	–
0.200	61.0°	81.17°	286.0	2.335 E-02	32.69
0.300	59.0°	76.88°	246.0	3.417 E-02	41.20
0.375	57.0°	73.76°	218.0	4.167 E-02	44.60
0.500	53.0°	68.78°	198.0	5.275 E-02	52.35

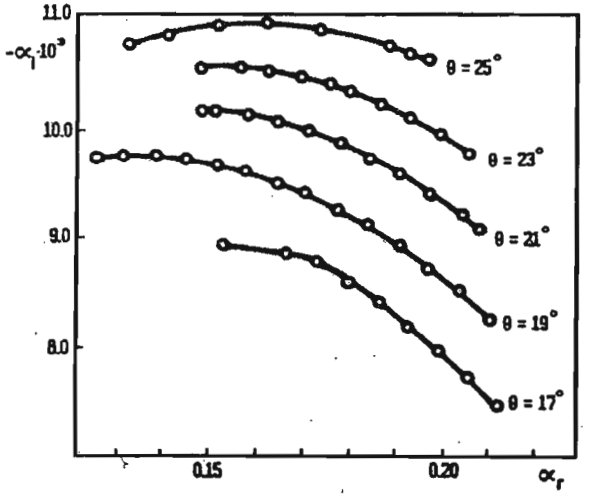

Fig. 9. Instability characteristics obtained for $Ma_e = 3.0$, $Re = 2000$, $\Omega/U_e = 0.375$, $\gamma = 60°$ and different cone angle

Fig.9 shows the influence of the cone angle Θ on the amplification rates of disturbances – the amplification rates increase with increasing Θ angle. When Θ reaches a value about 30° degrees, the structure of the vortices changes from counterrotating (Fig.1a) to corotating (Fig.1b). The vortex structure obtained for

$\theta = 15°$ is shown in Fig.10. In this figure the distributions of crossflow velocity perturbations CF' and perturbations of velocity component perpendicular to the wall v' are analyzed. Such a structure of disturbances imposes the intensive mixing of high and low velocities fluid. In section A–A the low velocity fluid from the lower half of the boundary layer is lifted up. At the same time high velocity fluid from the upper half of boundary layer (section B–B) is shifted down. In Fig.10b numerical results are compared with the sketch made by Kohama (1983) based on his experimental work.

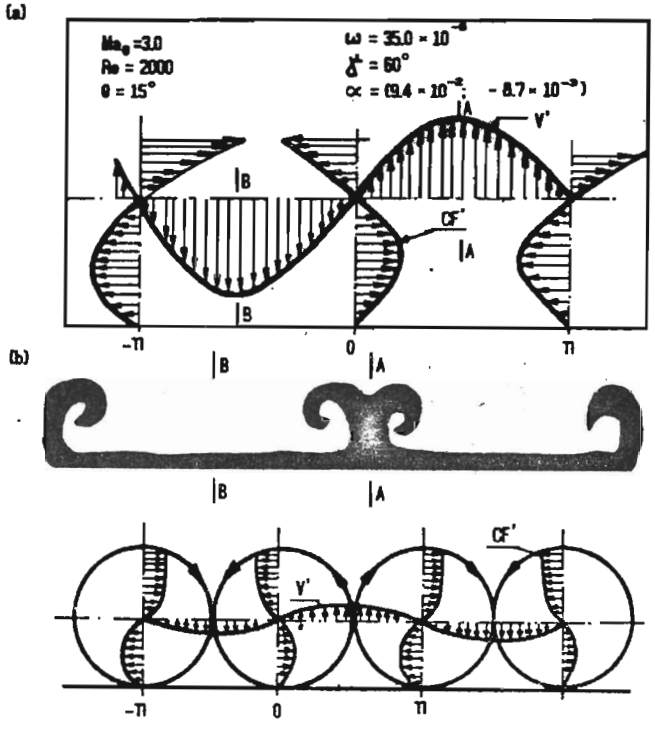

Fig. 10. (a) Distributions of crossflow perturbations CF' and perturbations of velocity component perpendicular to the wall v' – numerical results, (b) schematic picture of corotating vortices made by Kohama and Kobayashi (1983) based on his experimental work

5.2. Isothermal wall

The purpose of this part of work has been to estimate the effect of wall cooling on crossflow disturbances in supersonic boundary layer. The calculations

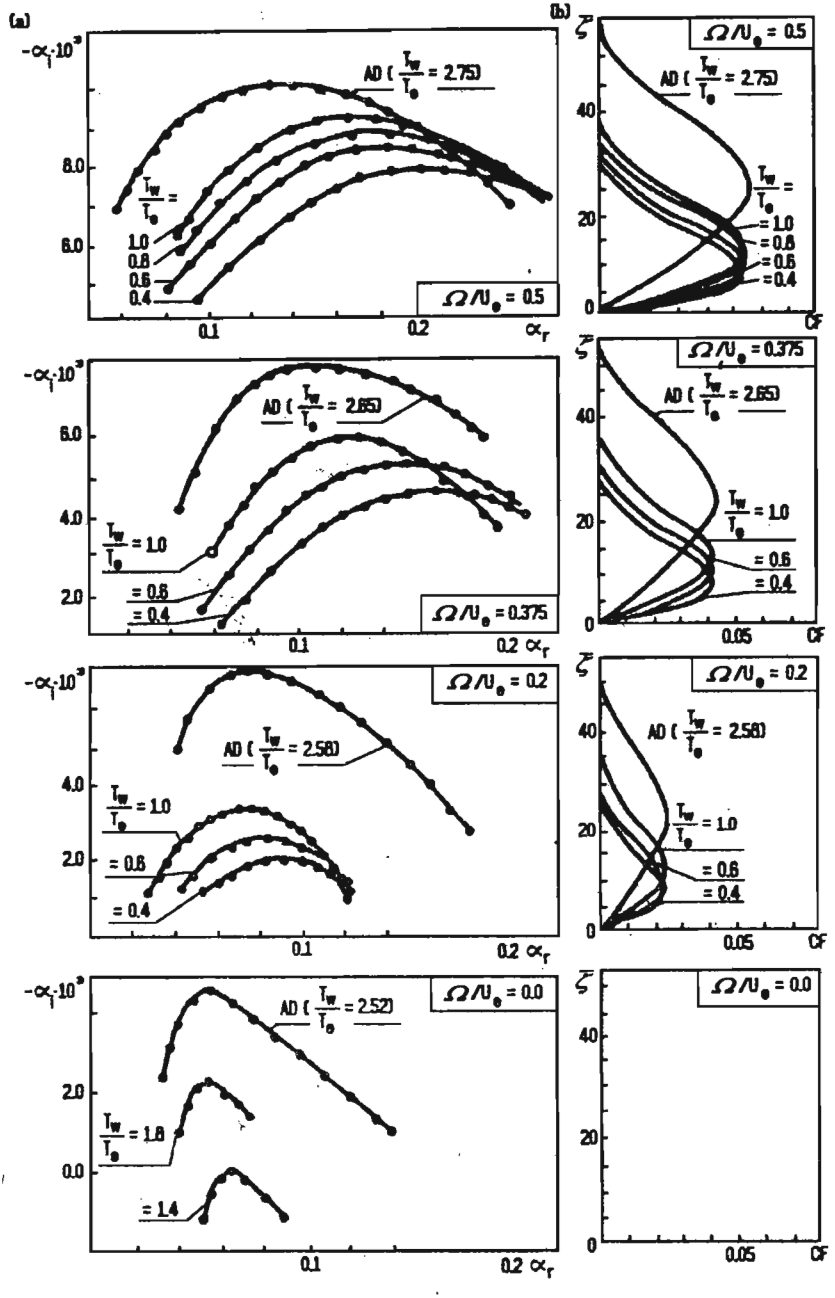

Fig. 11. Instability characteristics (a) and crossflow profiles (b) obtained for $Ma_e = 3.0$, $Re = 2000$, $\Theta = 15°$, different rotational speed $\Omega/U_e = 0.0$, 0.2, 0.375, 0.5 and different wall temperature conditions

were made for Reynolds number Re = 2000, cone angle $\theta = 15°$ and for the following combinations of rotational speed Ω/U_e, edge Mach number Ma_e and wall temperature condition T_w/T_e

Ω/U_e	Ma_e			T_w/T_e						
0.000	–	3.0	–	$AD(2.52)$	1.8	1.4	–	–	–	–
0.200	–	3.0	–	$AD(2.58)$	–	–	1.0	–	0.6	0.4
0.375	–	3.0	–	$AD(2.65)$	–	–	1.0	–	0.6	0.4
0.500	2.0	3.0	5.0	$AD(2.75)$	–	–	1.0	0.8	0.6	0.4

The results obtained for $\mathrm{Ma}_e = 3.0$ (the case where the second modes are not strongly amplified, cf Lees (1947)), Re = 2000 and for the different rotational speeds Ω/U_e are shown in Fig.11a. The rates of temperature for zero heat transfer condition (AD) are $T_w/T_e = 2.52,\ 2.58,\ 2.65,\ 2.75$ for the rotational speeds $\Omega/U_e = 0.0,\ 0.2,\ 0.375,\ 0.5$ respectively. The highest amplification rates were obtained for the rotational speed $\Omega/U_e = 0.5$ where the crossflow component is the largest one (Fig.11b) and the smallest for $\Omega/U_e = 0.0$ case (zero crossflow component). From Fig.11a we can see also that the amplification rates decrease with the lowering temperature rate.

The influence of wall cooling on crossflow profiles is shown in Fig.11b. We can see that the maximum values of crossflow profiles for particular rotational speeds are almost the same for all temperature boundary conditions. The important fact is that the wall cooling lowers the point of inflection and reduces the thicknes of the boundary layer.

The results obtained for $\mathrm{Ma}_e = 3.0$ are summarized in Fig.12 and Table 2 where critical Reynolds numbers versus wall temperature conditions are analyzed for different rotational speeds. As expected, the critical Reynolds number increases, for all rotational speeds, with the wall cooling. This confirms the supposition that the wall cooling stabilizes the crossflow disturbances. However, the wall cooling turned out to be most effective for the rest case where critical Reynolds number is 357 for zero heat transfer condition and 1946 for $T_w/T_e = 1.4$. From Fig.12 it is seen that the critical Reynolds number decreases with increasing rotational speed (with the increasing value of crossflow component) and for rotational speed $\Omega/U_e = 0.5$ the critical Reynolds number approaches almost the same value for all wall temperature conditions. The crossflow Reynolds number limit above which the wall cooling has turned out to be ineffective is 52.0 (Table 1).

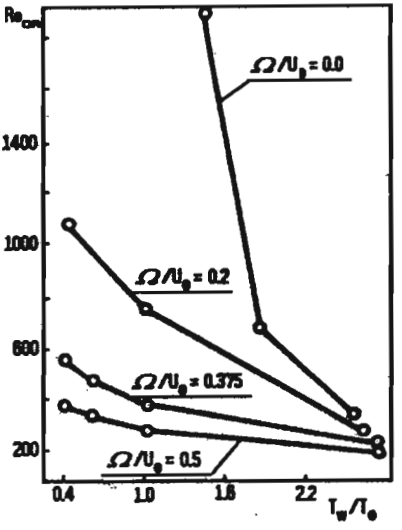

Fig. 12. Variations of the critical Reynolds number Re_{CR} against the wall temperature conditions for $Ma_e = 3.0$

Table 2. The variation of the critical Reynolds number Re_{CR} against temperature wall conditions T_w/T_e and rotational speeds Ω/U_e at edge Mach number $Ma_e = 3.0$ and Reynolds number $Re = 2000$

T_w/T_e / Ω/U_e	AD	1.8	1.4	1.0	0.8	0.6	0.4
0.000	357	678	1946	–	–	–	–
0.200	286	–	–	742	–	997	1070
0.375	218	–	–	390	–	482	548
0.500	198	–	–	296	305	344	382

To study the variations of the stability characteristics with the edge Mach number, the calculations were made at $Ma_e = 2.0, 3.0, 5.0$, at the rotational speed $\Omega/U_e = 0.5$ and the Reynolds number $Re = 2000$. The results are shown in Fig.13 for different wall temperature conditions. It is seen that the amplification rates of crossflow disturbances for $Ma_e = 5.0$ are much smaller compared to the case $Ma_e = 2.0$ and $Ma_e = 3.0$. It is the result of the dominant role of the second modes at so high Mach number (Fig.8). We can also see from Fig.13 that the stabilization effect of the wall cooling on crossflow disturbances in the case $Ma_e = 5.0$ and $\Omega/U_e = 0.5$ is minimal. Additionally we know that the wall cooling destabilizes the second modes.

We can conclude that in the cases in which second modes are not strongly

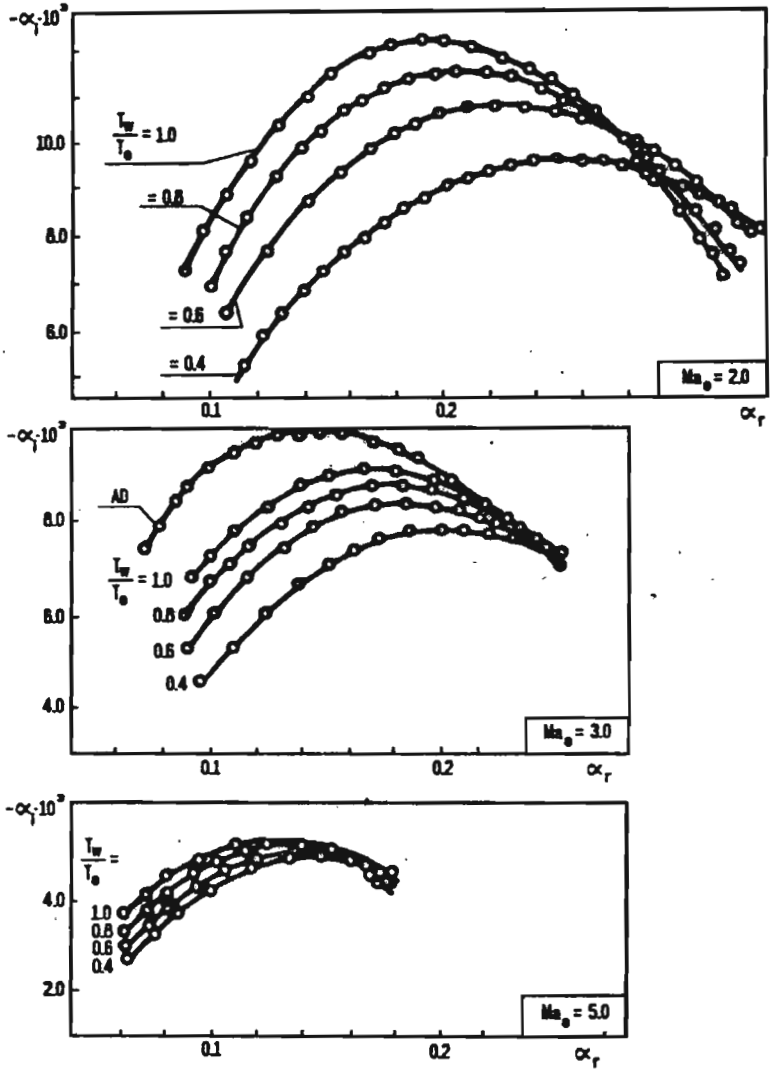

Fig. 13. Instability characteristics obtained for rotational speed $\Omega/U_e = 0.5$, Re = 2000, $\Theta = 15°$ and different edge Mach numbers and wall temperature conditions

amplified the wall cooling stabilizes the 3D-supersonic boundary layer but effectiveness of the wall cooling decreases with the increasing crossflow velocity component. The crossflow Reynolds number over which the wall cooling turned out to be ineffective is 52.

Acknowledgments

The author is most grateful to Prof. Walter Riess from the Unviversity of Hannover for allowing her to use the computer equipment.

References

1. BALACUMAR P., REED H., 1989, *Stability of three-dimensional supersonic boundary layer*, Report of Department of Mechanical and Aerospace Eng.

2. CEBECI T., BRADSHAW P., 1984, *Physical and computational aspects of convective heat transfer*, Springer Verlag, New York

3. GREGORY N., STUART J., WALKER W., 1955, *On the stability of three-dimensional boundary layers with applications to the flow due to a rotating disk*, Philos.Trans.R.Soc.London, Ser.A 248

4. ILLINGWORTH C., 1953, *The laminar boundary layer of a rotating body of revolution*, Phil.Mag., Ser.7, 44

5. KOBAYASHI R., 1981, *Linear stability theory of boundary layer along a cone rotating in axial flow*, Bull.Jpn.Soc.Mech.Eng., 24, 934-40

6. KOBAYASHI R., IZUMI H., 1983, *Boundary layer transition on a rotating cone in still fluid*, J.Fluid Mech., 127, 353-64

7. KOHAMA Y., KOBAYASHI R., 1983, *Behaviour of spiral vortices on rotating axisymmetric bodies*, The Report of the Institute of High Speed Mechanics, Tohoku University, Sendai, Japan, 47

8. LEES L., 1947, *The stability of laminar boundary layer in compressible fluid*, NACA R., 287

9. LEKOUDIS S., 1979, *The stability of the boundary layer on a swept wing with wall cooling*, AIAA Pap., 79-1495

10. MACK L., 1975, *Linear stability theory and the problem of supersonic boundary layer transition*, AIAA J., 13

11. MALIK M., CHUANG S., HUSSAINI M., 1982, *Accurate numerical solution of compressible linear stability equations*, ZAMP, 33, 189-201

12. OWEN P., RANDALL D., 1952, *Boundary layer transition on the swept wing*, RAE TM Aero., 277

13. SMITH N., 1946, *Exploratory investigation of laminar boundary layer oscillations on a rotating disk*, NACA TN-1227

Liniowa teoria niestabilności trójwymiarowej naddźwiękowej warstwy przyściennej

Streszczenie

W pracy badana jest, metodą numeryczną, niestabilność trójwymiarowej naddźwiękowej warstwy przyściennej powstałej na powierzchni stożka wirującego w przepływie jednorodnym. Do badań zastosowano teorię liniową. Przepływ podstawowy wyznaczany jest przy zastosowaniu transformacji Manglera i zmiennych podobieństwa. Równania liniowej teorii niestabilności rozwiązywane są metodą różnic skończonych. Obliczenia charakterystyk niestabilności przeprowadzono dla ścianki adiabatycznej i izentropowej. Badano wpływ chłodzenia na niestabilność naddźwiękowej warstwy przyściennej.

Manuscript received October 1, 1992; accepted for print December 1, 1992